First-principles calculation of the electronic structure, chemical bonding, and thermodynamic properties of β-US_2*

Li Shi-Chang(李世长)[a], Zheng Yuan-Lei(郑远蕾)[a], Ma Sheng-Gui(马生贵)[a], Gao Tao(高 涛)[a]†, and Ao Bing-Yun(敖冰云)[b]‡

[a] *Institute of Atomic and Molecular Physics, Sichuan University, Chengdu* 610065, *China*

[b] *Science and Technology on Surface Physics and Chemistry Laboratory, P. O. Box* 9071-35, *Jiangyou* 621907, *China*

(Received 7 July 2015; revised manuscript received 5 August 2015; published online 20 October 2015)

The electronic structure, magnetic states, chemical bonding, and thermodynamic properties of β-US_2 are investigated by using first-principles calculation through the density functional theory (DFT) $+U$ approach. The obtained band structure exhibits a direct band gap semiconductor at Γ point with a band gap of 0.9 eV for β-US_2, which is in good agreement with the recent experimental data. The charge-density differences, the Bader charge analysis, and the Born effective charges suggest that the U–S bonds of the β-US_2 have a mixture of covalent and ionic characters, but the ionic character is stronger than covalent character. The Raman-active, infrared-active, and silent modes at the Γ point are further assigned and discussed. The obtained optical-mode frequencies indicate that the three apparent LO–TO (longitudinal optical–transverse optical) splittings occur in B_{1u}, B_{2u}, and B_{3u} modes, respectively. Furthermore, the Helmholtz free energy ΔF, the specific heat ΔE, vibrational entropy S, and constant volume C_V are studied over a range from 0 K$\sim$100 K. We expect that our work can provide some valuable information for further experimental investigation of the dielectric properties and the infrared reflectivity spectrum of uranium chalcogenide.

Keywords: β-US_2, magnetization, chemical bonding, thermodynamic properties

PACS: 71.27.+a, 31.15.ae, 74.25.Bt **DOI:** 10.1088/1674-1056/24/12/127101

1. Introduction

The chalcogenide compounds of the actinides, especially of uranium, have attracted extensive attention because of their particular physical properties and their potential applications in nuclear fuels.[1] The β-US_2 has attracted much more attention because of its interesting subtle magnetic change.[2,3] However, the localized and strongly correlated 5f electrons in U material make experimental investigation and computational simulations of these materials challenging.

Recently, uranium disulfide (β-US_2), as a member of the class of strongly correlated materials, has been extensively studied experimentally because of its structural and magnetic properties.[2–7] Suski *et al.*[2] investigated the crystal structure of β-US_2 by using single crystal x-ray diffraction. Tateiwa *et al.*[3] measured the magnetization of β-US_2 under high pressure by piston cylinder and indenter-type cells in a superconducting quantum interference device (SQUID) magnetometer. Metoki and Ikeda,[4] and Metoki *et al.*[5] studied the metal–insulator crossover in β-US_2 by using spin polarized neutron scattering. Ikeda *et al.*[6] performed a high pressure study to investigate the insulator–semimetal transition in β-US_2. Yamamoto *et al.*[7] studied the magnetic behavior of β-US_2 based on the magnetic polaron model.

However, to our knowledge, some of the ground-state properties of β-US_2 are still unclear or under debate, and no data for phonon spectrum are available from the literature. As is well known, the accurate determination of phonon-dispersion curves is considered as an important reference for understanding its wide variety of physical properties of solids, such as: infrared, Raman, vibrational entropy, specific heats, Helmholtz free energy, internal energy, thermal expansion, constant volume heat capacity, lattice thermal conduction, and phenomena relating to the electron–phonon interaction. As a matter of fact, their understanding in terms of phonons is considered to be one of the most powerful pieces of evidence that our current quantum picture of solids is correct.[8,9] These wide interests require the theory and experiment to go hand in hand, and thus need reliable and accurate theoretical work.

Conventional density functional schemes that apply the local density approximation (LDA) or the generalized gradient approximation (GGA) fail to capture the localized characteristic of 5f electrons coming from the strong intra-atomic Coulomb interaction. One promising way to improve the drawback is the density functional theory (DFT) $+U$ approach, in which the underestimation of the strong electron–electron interaction is corrected by the Hubbard U parameter. Recently, a wide variety of physical properties of the uranium hydride, oxides, nitrides and carbides have been correctly reproduced by using LDA$+U$ or GGA$+U$ calculations.[10–13] However, systematic theoretical investigations of the struc-

*Project supported by the National Natural Science Foundation of China (Grant Nos. 21371160 and 21401173).

†Corresponding author. E-mail: gaotao@scu.edu.cn

‡Corresponding author. E-mail: aobingyun@caep.cn

© 2015 Chinese Physical Society and IOP Publishing Ltd

tural, magnetic and thermodynamic properties of the orthorhombic phase of US_2 (*Pbnm*, No. 62) are lacking. Consequently, according to the good performance of DFT+U approaches in describing the strong-correlation systems, we will carry out the present study on β-US_2 to provide a comparison with the experimental data currently available from the literature.

In this paper, we first investigate the electronic structure and magnetic stability of β-US_2 at the ground-state by using the first-principles approach to which the Hubbard parameter U and the spin-polarization are added. We will then calculate the charge–density difference in the (001) plane, the Bader charge analysis and the Born effective charges. In addition, optical-mode frequencies including Raman-active and the infrared-active modes at Γ point are discussed in detail. The thermodynamic functions, such as ΔF, ΔE, C_V, and S, are predicted in a range from 0 K to 1000 K.

The rest of the present paper is organized as follows. In Section 2, we introduce the theoretical framework and details of our calculations. In Section 3, we present and discuss the results of the electronic structure, chemical bonding, and thermodynamic properties of β-US_2. In Section 4, we summarize our main findings and draw some conclusions.

2. Computational method

In the present work, the calculations are performed by using the Vienna *ab initio* simulation package (VASP)[14] through employing the GGA (LDA) exchange and the projector augmented wave (PAW) method[15,16] to treat the core. The parameters for GGA (LDA) +U are set to be $U = 4.5$ eV and $J = 0.5$ eV, based on generally accepted values in the literature,[17,18] in VASP only their difference is meaningful, so the effective U is 4 eV. The uranium $5f^3 6s^2 6p^6 6d^1 7s^2$ and the sulfur $3s^2 3p^4$ electrons are treated as valence electrons. The self-consistent calculations are considered to be converged when the calculated total energy converges to less than 10^{-5} eV for all of the iterations. A kinetic energy cutoff of 550 eV is used for the set of plane waves, and the k-point meshes in the full Brillouin-zone (BZ) are sampled by $3 \times 4 \times 7$ k-mesh, and obtained by using the Monkhorst–Pack (MP) method.[19] Both spin-unpolarized and spin-polarized calculations are performed in this study. In the antiferromagnetic (AFM) calculations, we use the collinear $1-k$ AFM structure where the atomic spin moment is along the [001] direction.

The charge transfers between the uranium atoms and the sulfur atoms are determined by the Bader charge analysis,[20] which is based on the quantum theory of atoms in molecules (QTAIM). The Born effective charges are obtained not only to describe the change in macroscopic polarization but also to study the longitudinal optical (LO) and transverse optical (TO) splitting at Γ point. The phonon dispersions and phonon density of states (DOS) are calculated by using the linear-response method[21,22] that is implemented in the Phonopy software package,[23] which is based on density-functional perturbation theory (DFPT).

3. Results and discussion

3.1. Crystal structure and magnetic properties

Orthorhombic US_2 with the space *Pbnm* ($a = 8.480$ Å, $b = 7.114$ Å, and $c = 4.121$ Å), also called β-US_2, is a well known phase at room temperature. The unit cell is composed of four formula units (FU) with the uranium atoms in 4c (0.1228, 0.2477, 0.2500) Wyckoff sites, the sulfur atoms S1 in 4c (0.0664, 0.8561, 0.2500), and S2 in 4c (0.8338, 0.4710, 0.2500) Wyckoff sites, respectively (see Fig. 1).

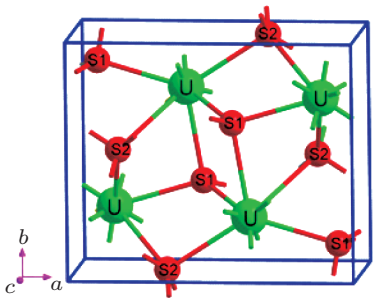


Fig. 1. (color online) The crystal structure of β-US_2. Green (big) balls stand for represent uranium atoms, and red (small) balls stand for refer to sulfur atoms.

Table 1 shows the calculated parameters for the nonmagnetic (NM), ferromagnetic (FM), and AFM states of β-US_2 by using GGA, LDA, GGA+U, and LDA+U methods. Both AFM and FM lattice constants from LDA+U typically underestimate experimental results whereas GGA+U overestimates the results. Root mean square (RMS) deviations in GGA+U lattice constants are similar for FM (0.088 Å) and AFM (0.088 Å) states of β-US_2, but slightly larger for FM (0.094 Å) and AFM (0.095 Å) states in LDA + U method. We do not report GGA (LDA) results for the RMS data because they fails to reach the right ground state for the strongly correlated system, which predicts β-US_2 to be an incorrect conductor.

The values of relative total energy $E_{\text{rel.}}$ (eV per β-US_2) for the states of NM, FM, and AFM phases are calculated as listed in Table 1. We find that the total energies of the NM phase are both the highest in the GGA (LDA) scheme with and without Coulomb interaction; in other words, the NM phase is unstable for β-US_2. According to the small value of total energy difference ΔE between FM and AFM states within the GGA (LDA)+U approaches, β-US_2 is expected to have a paramagnetic phase,[24] and the FM and AFM states could be degenerate, which is consistent with the available experimental results.[6]

Table 1. Calculated and experimental results for β-US_2: optimized lattice constants, total magnetic moment μ_{tot}, and band gaps Δ. Calculated relative energy $E_{rel.}$ (eV per β-US_2) for NM, FM, and AFM *Pbnm* β-US_2. (EMS^2=$\frac{1}{3}[(a-a_{exp.})^2+(b-b_{exp.})^2+(c-c_{exp.})^2]$).

Method	Magnetism	a_0/Å	b_0/Å	c_0/Å	μ_{tot}/μ_B	E_{gap}/eV	$E_{rel.}$/eV	EMS
GGA	NM	8.394	7.041	3.941	–	0.0	0.88	–
	FM	8.466	7.033	4.044	7.448	0.0	0.36	–
	AFM	8.498	7.124	3.998	0.000	0.0	0.00	–
GGA+U	NM	8.687	7.147	3.996	–	0.0	2.53	–
	FM	8.590	7.199	4.185	7.900	0.6	0.00	0.088
	AFM	8.587	7.201	4.186	0.000	0.9	0.01	0.088
LDA	NM	8.215	6.904	3.841	–	0.0	0.54	–
	FM	8.243	6.909	3.909	6.876	0.0	0.00	–
	AFM	8.233	6.973	3.844	0.000	0.0	0.32	–
LDA+U	NM	8.368	7.025	3.888	–	0.0	1.80	–
	FM	8.383	7.022	4.028	7.896	0.2	0.00	0.094
	AFM	8.381	7.018	4.030	0.000	0.4	0.01	0.095
Exp.[a)]		8.480	7.114	4.121		1.2		

[a]Ref. [2].

Overall, comparing our theoretical predictions with the experimental results, the accuracy of our atomic-structure and band-gap prediction for β-US_2 is found to be quite satisfactory by tuning the effective Hubbard parameter within the GGA+U approach of the AFM phase (the paramagnetic phase is unavailable in the present code), which supplies the safeguard for our further study of the electronic properties and chemical bonding nature of β-US_2.

3.2. Electronic properties: Band structure and density of states

The calculated band structures of β-US_2 along Γ-Y-T-Z-Γ-X-S-R-U directions in the full BZ are shown in Fig. 2. Here, the high-symmetry points correspond to Γ(0, 0, 0), Y(1/2, 0, 0), T(0, 1/2, 1/2), Z(0, 0, 1/2), S(1/2, 1/2, 0), X(0, 1/2, 0), R(1/2, 1/2, 1/2), and U(1/2, 0, 1/2). The Fermi energy is assumed to be at a zero level. Figure 2 shows a direct band gap with a width of 0.9 eV at $U = 4.5$ eV within GGA+U approach, which is well consistent with the available experimental value of 1.2 eV. The first valence bands are presented in an energy region from 5.3 eV to Fermi energy level. The second valence bands are located at 11 eV below the Fermi energy level, with a width of about 2.5 eV (which is not shown in Fig. 2).

The total densities of states (TDOSs) and their corresponding partial densities of states (PDOSs) of U and S atoms for β-US_2 are shown in Fig. 3. We can see that the d orbitals and f orbitals of U atom contribute less to their valence bands, while the f orbitals of U atom mainly contribute to the conduction bands. The upper valence band is mainly contributed from S-3p orbital with an admixture of U-5f orbital, revealing that a hybridization between the U and S atoms ranges from the −1.5 eV to −3.5 eV. The U-6d states also make some contributions to the hybridization. However, the hybridization between U-5f and the S-3p is weak, indicating that more ionicity character exists in the bonds. This feature can also be confirmed by following chemical bonding analysis.

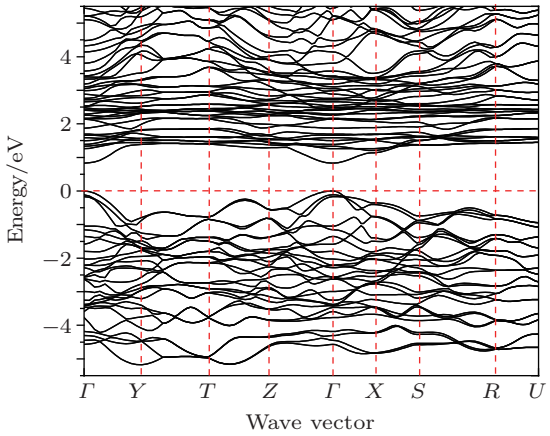


Fig. 2. (color online) Calculated band structure for β-$US_2$by using GGA+U. The Fermi level is at 0 eV.

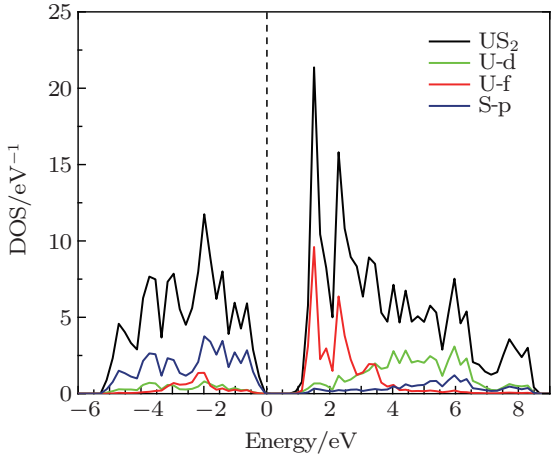


Fig. 3. (color online) Calculated total density of states (TDOSs) and partial density of states (PDOSs) for β-US_2 by using GGA+U. The Fermi level is at 0 eV.

3.3. Chemical bonding

In order to analyze the U–S bonding of β-US_2, we plot the charge–density contour maps (in units of e/Å^3) along the (001) plane, as shown in Fig. 4(a). For each U atom, the charge is the sum of the charges of 14 electrons outside the core of the PAW potential and the core states are occupied by 78 electrons. It can be clearly seen that the highest density charge piles up in the immediate vicinity of the nuclei, while the interstitial charge densities are relatively low. This reflects that most of the electrons are firmly bound up around the atomic nuclei and only a few valence electrons can escape from their bondage.

To understand the extent of charge transfer accompanying the formation of uranium chalcogenide compounds, we also plot the charge density difference contour maps by the following equation:[25]

$$\delta\rho = \rho(US_2) - \rho(U) - \rho(S), \tag{1}$$

where ρ is the valence-electron charge density. The result in the (001) plane is displayed in Fig. 4(b), the blue zone and orange zone represent the loss of charge and the gain of charge, respectively. For each calculation, we use the $2\times2\times1$ supercell with the nuclear positions and lattice parameters fixed at the same values. By examining the plotted actual charge–density difference it is found that there is net charge transfer from the U atom to the S atom, while there is also obvious charge accumulation in the interstitial regions of U and S atoms. Thus, the U–S bond can be described as a mixture of covalent and ionic components. Moreover, one can also see that there is more charge transfer from U to S1 than from U to S2, which indicates that the ionic character of U–S1 is stronger than U–S2.

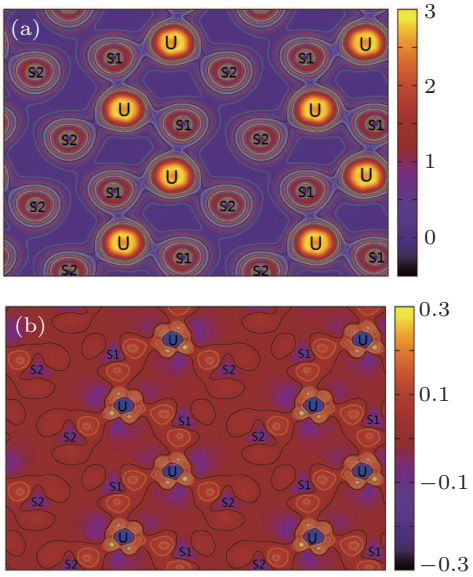


Fig. 4. (color online) Calculated (a) charge density and (b) charge density difference contour plots from the GGA+U calculation for β-US_2 (in the units of e/Å^3) alone the (001) plane.

Combined with the orbital-resolved PDOSs shown in Fig. 2, we find that the ionicity character of the U–S bond can be attributed to the charge transfer from U-5f and U-6d states to S-3p states, and the covalent character of the U–S bond is associated with the hybridization between U-5f and S-3p states.[26,27]

Table 2. Calculated Bader charges (Q_B) and Bader volumes (V_B) for AFM/FM β-US_2 by GGA+U.

Method	Magnetism	Q_B(U)/e	Q_B(S_1)/e	Q_B(S_2)/e	V_B(U)/Å^3	V_B(S_1)/Å^3	V_B(S_2)/Å^3
GGA+U	FM	11.86	7.10	7.04	19.43	21.18	23.94
	AFM	11.86	7.10	7.04	19.44	21.26	24.01

To further quantify the charge transfer between the U atom and the S atom, we perform a Bader charge analysis[28] of the charge density. In this calculation, we use a $128\times108\times64$ charge density grid for the unit cell. The competition between the ionic character and covalent character in β-US_2 can be related to the charge transfer between U atom and S atom. From Table 2, we can find that each U atom loses $2.14|e|$, while a charge of $1.10|e|$ is transferred to S1 atom and $1.04|e|$ transfer to S2 atom. These estimates suggest that any directional bonding of the S atom to U atom is ionic and small. Meanwhile, the results illustrate that the S1 atoms in β-US_2 are easier to gain electrons than S2 atoms; in other words, the ionic character of U–S1 is stronger than U–S2.

Furthermore, we also calculate the Born effective charges to describe the charge in macroscopic polarization that is created by collective atomic displacements. In Table 3, Z_j^* ($j=1$, 2, 3) is the j-th eigenvalue of symmetric part of the Z^* tensor and $\bar{Z}$ is the average of eigenvalue. The Born effective charges of S1 (-2.80 a.u.) is very close to its nominal ionic valence charge (-2 a.u.) and, therefore, U–S1 is considered to have almost the ionic character, which is similar to the result of charge–density difference and Bader charge analysis as mentioned above.

Table 3. Born effective charges of β-US_2.

Method	Magnetism		Z_1^*	Z_2^*	Z_3^*	$\bar{Z}$
GGA+U	AFM	U (4c)	5.67	5.60	6.04	5.77
		S_1 (4c)	–3.24	–2.47	–2.69	–2.80
		S_2 (4c)	–2.49	–3.13	–3.41	–3.01

By comparing the charge–density difference, the Bader charge analysis and the Born effective charge for β-US_2, we

can find that: (i) mixtures of covalent and ionic character are present in both U–S1 bond and U–S2 bond, but the ionic character is slightly stronger than the covalent character, and when compared with scenario of U–S2 bond, the ionicity character of the U–S1 bond is slightly stronger than covalent character; and, (ii) the ionic charges for AFM and FM β-US_2 can both be represented as $U^{+2.14}S_1^{-1.10}S_2^{-1.04}$ by GGA$+U$ calculations.

3.4. Phonon and thermodynamic properties

The phonon spectrum is closely associated with the dynamic stability, lattice thermal conduction, and thermodynamic properties of solid at finite temperature. In this work, the phonon spectra of the β-US_2 are calculated by density-functional perturbation theory (DFPT) with GGA$+U$ scheme for its AFM state. The calculated phonon dispersion curves and phonon DOS are plotted in Fig. 5.

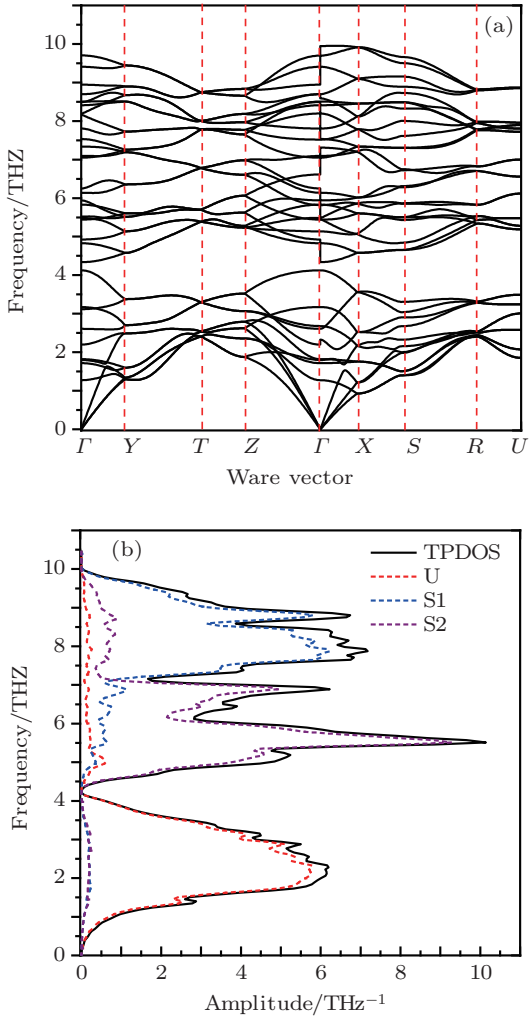


Fig. 5. (color online) The calculated phonon dispersion curves by LO–TO splitting β-US_2. (a) phonon dispersion curves and (b) phonon TDOS and PPDOS.

As shown in Fig. 1, each unit cell of β-US_2 contains 12 atoms. Therefore, this system contains 36 normal modes, three of them are in the acoustic modes and the remainders are in optical modes. Since the space group of β-US_2 is *Pnma* (No. 62), the corresponding point group is D_{2h} (*mmm*). Based on the group-theoretical analysis, the irreducible representations of the vibrational modes in the center of the BZ can be expressed as follows:

$$\begin{aligned}\Gamma_{\text{acoustic}} &= \mathrm{B_{1u}}+\mathrm{B_{2u}}+\mathrm{B_{3u}},\\ \Gamma_{\text{optic}} &= 6\mathrm{A_g}+3\mathrm{A_u}+6\mathrm{B_{1g}}+2\mathrm{B_{1u}}\\ &\quad +3\mathrm{B_{2g}}+5\mathrm{B_{2u}}+3\mathrm{B_{3g}}+5\mathrm{B_{3u}}.\end{aligned}$$

Among them, 12 modes ($2B_{1u}$, $5B_{2u}$ and $5B_{3u}$) are infrared active, 18 modes ($6A_g$, $6B_{1g}$, $3B_{2g}$, and $3B_{3g}$) are Raman active, while the remaining three optical modes ($3A_u$) are Silent modes.

In order to investigate the polarization effects of β-US_2, we calculate the macroscopic static dielectronic tensor (including local field effects in DFT) and the Born effective charge tensor to correctly account for the longitudinal optical (LO)-transverse optical (TO) splitting at the Γ point for each nonequivalent atom based on DFPT. The calculated diagonal elements of the macroscopic static dielectric tensor are $\varepsilon_0^{xx}=10.964$, $\varepsilon_0^{yy}=10.998$, and $\varepsilon_0^{zz}=11.723$, respectively.

The calculated phonon dispersion curves of *Pbnm* phase along high symmetry points in the BZ and the corresponding phonon DOS are shown in Fig. 5. We can see that the calculated phonon dispersion curves have no soft mode in the whole Brillouin zone at ambient pressure and 0 K, which indicates that β-US_2 is dynamically stable.

Figure 5(b) also shows the PPDOSs projected onto U, S1, and S2 atoms. Owing to the fact that the U atom is heavier than the S atom, the vibration frequency of the U atom is lower than that of the S atom. Therefore, a gap exists between the optic branch and the acoustic branch. In the overall view of Fig. 5(b), one can find that there are three frequency ranges: the lowest part is from 0 THz to 4.1 THz, which is main contribution coming from the U atom; the middle part is from 4.4 THz to 7.0 THz dominated by the S2 atom; and, the highest part is from 7.0 THz to 10.0 THz, which is strongly related to the S1 atom.

The calculated phonon frequencies at the Γ point are listed in Table 4, including Infrared, Raman, and Silent active modes with LO–TO splitting. It is commonly believed that the LO–TO splittings are different for all modes, only the Infrared-active modes show the largest TO–LO splitting, while Raman and Silent active modes do correspond to modes of small or zero LO–TO splitting.[29] The results of our calculation also indicate that the LO–TO splittings of Infrared-active modes are apparent but there is no splitting in the Raman active mode nor Silent active mode. Since the B_{1u} mode has displacement along the z axis, B_{2u} mode has displacement along the y axis, the LO–TO splitting for displacement parallel

to z-principal axis occurs for the B_{1u} mode and displacement parallel to y axis occurs for the B_{2u} mode. Large frequency splittings occur in B_{1u} (144.7 cm^{-1}–220.6 cm^{-1}) and B_{2u} (194.1 cm^{-1}–245.7 cm^{-1}) modes, which suggests that they involve large effective charges and make large contributions to the static dielectric tensor. The apparent LO–TO splitting indicates that β-US_2 is a polar material.

Table 4. Optical phonon frequencies (in unit cm^{-1}) and LO–TO splitting for infrared active modes at Γ point of β-US2. R represents Raman active, IR denotes infrared active. The first column ($e = 0$) is for no electric field, the $e \parallel x$, $e \parallel y$, and $e \parallel z$ are for the fields parallel to x, y, and z principal axis, respectively. $\Delta\omega^2 = \Delta\omega^2_{LO} - \Delta\omega^2_{TO}$.

	Modes	$e=0$	$e \parallel x$	$e \parallel y$	$e \parallel z$	$\sqrt{\Delta\omega^2}$
Infrared (IR)	$B_{1u}(1)$	144.7	144.7	144.7	220.6	166.5
	$B_{1u}(2)$	251.3	251.3	251.3	290.1	144.9
	$B_{2u}(1)$	89.4	89.4	104.0	89.4	53.1
	$B_{2u}(2)$	171.3	171.3	184.1	171.3	67.4
	$B_{2u}(3)$	194.1	194.1	245.7	194.1	150.6
	$B_{2u}(4)$	250.8	250.8	272.1	250.8	105.5
	$B_{2u}(5)$	323.5	323.5	323.7	323.5	11.4
	$B_{3u}(1)$	73.3	77.7	73.3	73.3	25.8
	$B_{3u}(2)$	164.3	181.6	164.3	164.3	77.4
	$B_{3u}(3)$	208.4	243.8	208.4	208.4	126.5
	$B_{3u}(4)$	283.3	286.5	283.3	283.3	41.5
	$B_{3u}(5)$	298.3	331.8	298.3	298.3	145.3
Raman(R)	$A_g(1)$	59.9				
	$A_g(2)$	87.0				
	$A_g(3)$	183.1				
	$A_g(4)$	204.7				
	$A_g(5)$	273.4				
	$A_g(6)$	290.1				
	$B_{1g}(1)$	105.8				
	$B_{1g}(2)$	137.6				
	$B_{1g}(3)$	198.1				
	$B_{1g}(4)$	236.7				
	$B_{1g}(5)$	260.3				
	$B_{1g}(6)$	313.9				
	$B_{2g}(1)$	57.2				
	$B_{2g}(2)$	194.5				
	$B_{2g}(3)$	283.7				
	$B_{3g}(1)$	60.7				
	$B_{3g}(2)$	181.6				
	$B_{3g}(3)$	280.5				
Silent	$A_u(1)$	42.5				
	$A_u(2)$	161.0				
	$A_u(3)$	235.2				

Based on phonon DOS, the thermodynamic properties, such as the phonon contributions to the internal energy ΔE, the Helmholtz free energy ΔF, entropy S, and the constant-volume specific heat capacity C_V, can be obtained by using the standard quasiharmonic approximation.[30] Within the approximation, the ΔE, ΔF, S, and C_V can be given through

$$\Delta E = 3nN\frac{\hbar}{2}\int_0^{\omega_L} \omega \coth\left(\frac{\hbar\omega}{2k_BT}\right) g(\omega)\,\mathrm{d}(\omega), \quad (2)$$

$$\Delta F = 3nNk_BT\int_0^{\infty} \ln\left\{2\sinh\left(\frac{\hbar\omega}{2k_BT}\right)\right\} g(\omega)\,\mathrm{d}(\omega), \quad (3)$$

$$S = 3nN\frac{\hbar}{2}\int_0^{\omega_L}\left[\frac{\hbar\omega}{2k_BT}\coth\frac{\hbar\omega}{2k_BT} - \ln\left\{2\sinh\frac{\hbar\omega}{2k_BT}\right\}\right] g(\omega)\,\mathrm{d}(\omega), \quad (4)$$

and

$$C_V = 3nN\frac{\hbar}{2}\int_0^{\omega_L}\left(\frac{\hbar\omega}{2k_BT}\right)^2 \mathrm{csch}^2\left(\frac{\hbar\omega}{2k_BT}\right) g(\omega)\,\mathrm{d}(\omega), \quad (5)$$

respectively.

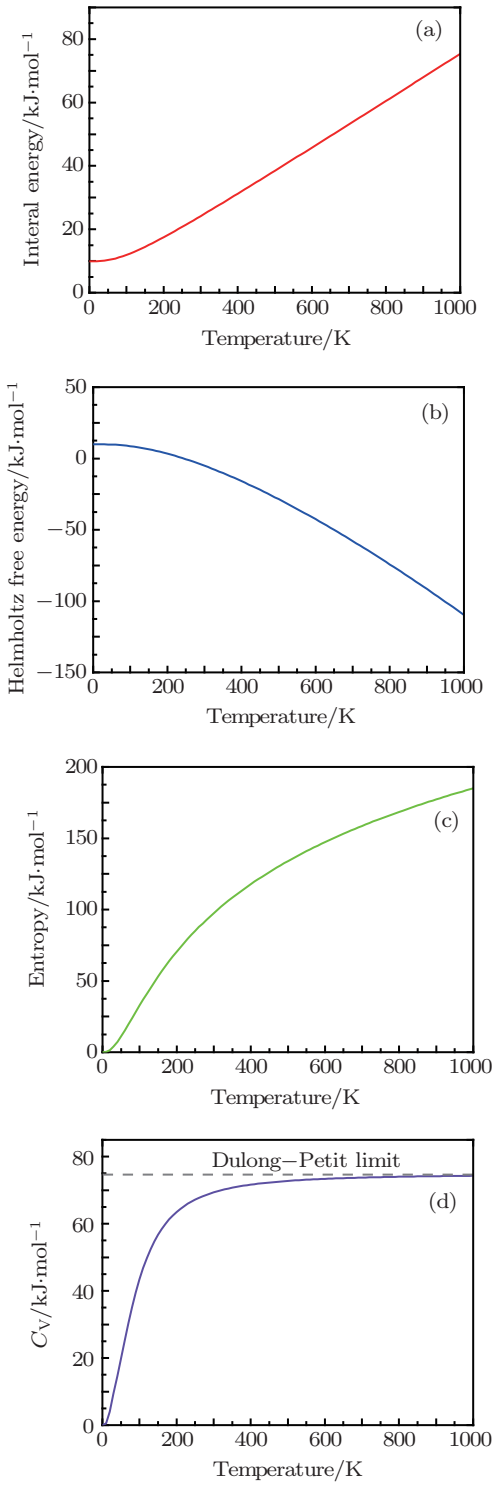


Fig. 6. (color online) Calculated thermodynamic properties of β-US_2. (a) the internal energy ΔE, (b) the Helmholtz free energy ΔF, (c) the entropy S, (d) the constant-volume specific heat C_V.

Where k_B and $\hbar$ are the Boltzman constant and the number of atoms per unit cell, respectively; ω is the phonon frequencies; N is the number of unit cell; and, $g(\omega)$ is the normalized phonon DOS.

The curves of calculated internal energy ΔE, the Helmholtz free energy ΔF, the entropy$S$ and the constant-volume specific heat C_V versus temperature in a range from 0 K to 1000 K are shown in Fig. 6. The variation of C_V with temperature obeys the Debye T^3 law at low temperature, while over 500 K, C_V they are close to the classic limit (which is called Dulong–Petit's law). To our knowledge, experimental and theoretical studies of the thermodynamic properties of β-US_2 have not been found. Thus we hope that our results can guide future experimental investigations on the thermodynamic properties of β-US_2

4. Conclusions

In this work, we present systematic studies of the electronic structure, chemical bonding, and thermodynamic properties of β-US_2 in its orthorhombic lattice by using first-principles calculation with the LDA, GGA, LDA$+U$, and GGA$+U$ approaches. By comparing with available experimental results, we find that Coulomb repulsion is vitally important. The correct ground-states of the paramagnetic phase β-US_2 reported in experiments[6] are successfully reached by the GGA$+U$ method. The calculations begin with the optimization for the lattice parameters and atomic coordinates. The results show that the calculated structural parameters and atomic coordinates are consistent with the experimental values. The calculated band structure and DOS indicate that β-US_2 is a direct gap semiconductor with a wide gap of 0.9 eV.

On the basis of the electronic structure investigations, we also carry out systematic studies of chemical bonding and the dynamical properties of β-US_2. By investigating the charge density differences, the Bader charge and the Born effective charges, we find that both U–S1 and U–S2 bond can be described as a mixture of covalent and ionic components but the ionic character is stronger than covalent character. The ionicity character of the U–S1 bond is slightly stronger than that of the U-S2 bond. The Raman and infrared active frequencies are assigned and presented. In particular, the infrared active modes are discussed in detail by LO–TO splitting. We can observe three giant LO–TO splittings occurring in B_{1u}, B_{2u}, and B_{3u} modes. Finally, the thermodynamic properties are studied, such as ΔF, ΔE, C_V, and S in temperatures ranging from 0 K to 1000 K within the harmonic approximation. We expect that our work can provide some valuable information about uranium chalcogenide compound materials that can be used for further experimental investigations.

Acknowledgment

The authors are grateful to the Center of High Performance Computing at the physics discipline of Sichuan University for their assistance with our computing needs.

References

[1] Kohlmann H and Beck H P 1997 *Z. Anorg. Allg. Chem.* **632** 785
[2] Suski W, Gibiński T, Wojakowski A and Czopnik A 1972 *Phys. Stat. Solidi* **9** 653
[3] Tateiwa N, Haga Y, Sakai H, Ikeda S, Matsuda T D, Yamamoto E and Onuki Y 2011 *J. Phys. Soc. Jpn.* **80** SA103
[4] Metoki N and Ikeda S 2013 *J. Korean Phys. Soc.* **62** 1782
[5] Metoki N, Sakai H, Suzuki M, Yamamoto E, Haga Y, Matsuda T D and Ikeda S 2014 *J. Phys. Soc. Jpn.* **3** 013011
[6] Ikedaa S, Sakaia H, Matsudaa T D, Tateiwaa N, Nakamuraa A, Yamamotoa E, Aokib D, Hommab Y, Shiokawab Y, Hedoc M, Uwatokoc Y, Hagac Y and Ounki Y 2008 *Physica B* **403** 893
[7] Yamamoto E, Tateiwa N, Haga Y, Ikeda S, Sakai H, Onuki Y and Fisk Z 2014 *J. Phys. Soc. Jpn.* **3** 011095
[8] Yu Y, Zhou J J, Han H L, Zhang C Y Cai T, Song C Q and Gao T 2009 *J. Alloys Compd.* **471** 492
[9] Baroni S, Gironcoli S D, Corso A D and Giannozzi P 2001 *Rev. Mod. Phys.* **73** 515
[10] Zhang Y, Wang B T, Lu Y, Yang Y and Zhang P 2012 *J. Nucl. Mater.* **430** 137
[11] Wang B T, Zhang P, Lizarraga R, Marco I D and Eriksson O 2013 *Phys. Rev. B* **88** 104107
[12] Lu Y, Wang B T, Li R W, Shi H L and Zhang P 2010 *J. Nucl. Mater.* **406** 218
[13] Shi H L, Zhang P, Li S S, Sun B and Wang B T 2009 *Phys. Lett. A* **373** 3577
[14] Kresse G and Hafner J 1993 *Phys. Rev. B* **47** 558
[15] Bloechl P E 1994 *Phys. Rev. B* **50** 17953
[16] Kresse G and Joubert D 1999 *Phys. Rev. B* **59** 1758
[17] Wang B T, Shi H, Li W and Zhang P 2010 *Phys. Rev. B* **81** 045119
[18] Wen X D, Martin R L, Scuseria G E, Rudin S P, Batista E R and Burrell A K 2013 *J. Phys.: Condens. Matter* **25** 025501
[19] Monkhorst H J and Pack J D 1976 *Phys. Rev. B* **13** 5188
[20] Bader R F W 1990 *Atoms in molecules: a uantum theory* (New York: Oxford University Press)
[21] Giannozzi P and de Gironcoli S 1991 *Phys. Rev. B* **43** 7231
[22] Gonze X and Lee C 1997 *Phys. Rev. B* **55** 10355
[23] Togo A, Oba F and Tanaka I 2008 *Phys. Rev. B* **78** 134106
[24] Huang L F, Zheng X H, Zhang G R, Li L L and Zeng Z 2011 *J. Phys. Chem. C* **115** 21088
[25] Hector L G, Herbst J F and Capehart T W 2003 *J. Alloys Compd.* **353** 74
[26] Wang B T, Shi H L, Li W D and Zhang P 2010 *Phys. Rev. B* **81** 045119
[27] Andersson D A, Lezama J, Uberuaga B P, Deo C and Conradson S D 2009 *Phys. Rev. B* **79** 024110
[28] Tang W, Sanville E and Henkelman G 2009 *J. Phys.: Condens. Matter* **21** 084204
[29] Iliev M N, Lee H G, Popov V N, Abrashev M V, Hamed A, Meng R L and Chu C W 1997 *Phys. Rev. B* **56** 2488
[30] Siegel A, Parlinski K and Wdowik U D 2006 *Phys. Rev. B* **74** 104116